Cracking due to leaching in cementitious composites: experimental investigation by means of X-ray microtomography and numerical modeling

T. Rougelot, N. Burlion
Laboratoire de Mécanique de Lille, UMR CNRS 8107, Villeneuve d'Ascq, France

D. Bernard
Institut de Chimie de la Matière Condensée de Bordeaux, UPR CNRS 9048, Pessac, France

F. Skoczylas
Laboratoire de Mécanique de Lille, UMR CNRS 8107, Villeneuve d'Ascq, France

ABSTRACT: Chemical degradation of cement based materials leads to significant degradation of their physical properties. A typical scenario is a calcium leaching due to water (water with very low pH compared with that of porous interstitial fluid). The main objective of this paper is to evaluate the evolution of microstructure induced by leaching of a cementitious composite using synchrotron X-ray microtomography, in the particular way of identification of cracking induced by leaching. After a brief description of the degradation mechanism and the X-ray synchrotron microtomographic analysis, we propose a numerical simulation performed in order to prove that cracking due to leaching is induced by an initial pre-stressing of concrete. This pre-stressing is due to endogenous shrinkage. After leaching, the tensile strength of cement paste is dramatically reduced leading to microcracking.

1 INTRODUCTION

Mortars and concretes are non-homogeneous materials whose macroscopic physical properties depend on their local characteristics. For instance, porosity and permeability of concrete are intimately related to the microstructure. Hence it is of importance to link local and macroscopic scale in order to study and model the mechanical behaviour and the transport properties of cementitious materials. This requires the knowledge of the 3D micro-geometry. In order to visualize this microstructure, various innovative techniques are currently developed such as acoustic emission analysis, infrared thermography or X-ray computed microtomography (XCMT).

Synchrotron XCMT finds applications in the study of sample microstructure without damaging it. The principle, similar to the medical scanner, consists of acquiring digital images of the material's X-ray absorption. This acquisition is undertaken at various angles: a three-dimensional image is then obtained by numerical reconstruction from the set of 2D-images.

Concrete leaching is often the result of a fluid attack (pure water or water with very low pH compared to that of the pore fluid), and leads to the hydrolysis of cement paste hydrates, important increase in porosity and permeability, and important decrease in mechanical properties. Existing models often use a damage behaviour in order to capture the main mechanical characteristic of the leached material. Using synchrotron XCMT as a non-destructive characterization method under accelerated leaching with ammonium nitrate solution leads to possible microtomographic analysis on the same specimen during the dissolution. It is then possible to determine the degradation kinetics, the leaching front position and the porosity increase without interfering with the material (Burlion et al. 2006). It is also possible to show cracking of material during the process. The cementitious materials containing aggregates (or glass spheres in the present case) are auto-stressed materials: indeed, the endogenous shrinkage of the cementing matrix causes a contraction around these aggregates. This contraction remains generally limited to values lower than the cement tensile strength. On the other hand, in the particular case of leaching, chemical attack will lead to a drastic decrease of tensile strength of the matrix. A micro-cracking will appear mainly around the aggregates, what results in a very notably weakening of the mechanical capacities of the material. As regards confirmation or not of these assumptions, a numerical study was led. It aims to highlight the preferential areas of cracks nucleation, by the use of a finite element code in nonlinear mechanics. The selected model has been chosen for its simplicity, and constitutes a first numerical approach of mechanical behaviour modelling of leached samples.

First we will briefly describe mortar degradation mechanism, and the principles of synchrotron X-ray computed microtomography. In a second part, we propose a numerical simulation of mortar leaching: the results obtained are described, demonstrating the capacity of the method to validate our hypothesis about the concrete cracking during leaching.

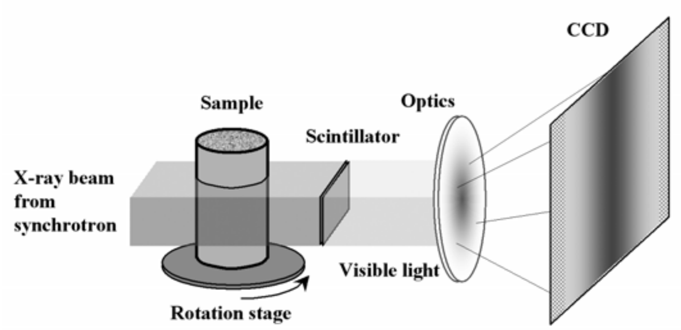

Figure 1. Sketch of the experimental setup for microtomography mapping.

2 EXPERIMENTAL TOOLS AND MEASUREMENTS

2.1 *X-ray microtomography used for leaching analysis*

High resolution microtomographic acquisitions were performed on the BM05 beam line of the European Synchrotron Radiation Facility (ESRF, Grenoble, France). In our case a monochromatic beam with energy of *30 keV* was used. The mortar sample was mounted on a rotative table and the acquisition consisted in the recording of 900 two-dimensional (2D) radiographs at equally spaced angles between 0° and 180° (Figure 1). A scintillator is set behind the sample to convert, as efficiently as possible, X-rays to visible light. Contrast obtained on the 2D projections results from the difference in X-ray absorption by the phases/features encountered by X-rays in the specimen. A mirror and the optical set-up selected for the experiment directs the light to the detector. The FRELON CCD camera, developed at ESRF, comprises *2048 x 2048 pixels*. A pixel size of $5.1x5.1\ \mu m^2$ is then obtained. The 2D radiographs were then exploited to reconstruct the volume of the samples using a conventional filtered backprojection algorithm.

2.2 *Material choice and specimens design and Accelerated leaching process*

The size of the sample was imposed by the microtomographic analysis. The maximal size was of 2048 x 5.1 μm (about 10 mm). Cylindrical cores of 8 mm diameter have been directly obtained from classical prism 40x40x160 mm^3 (Figure 2). Their lengths varied between 20 to 30 mm. To perform this study, different cementitious composites have been done: the key idea has been to reproduce cementitious composites initially proposed by Bisschop and van Mier to study effects of drying on microcracking (Bisschop & van Mier 2002, Shiotani et al. 2003). We will focus here only on a composite constituted with 35 % of glass spheres completed by with 35 % of glass spheres completed by a cement paste (cement CEM II/B 32,5R with water by cement ratio equal to 0.5). The glass sphere diameter is 2 mm. Furthermore, a sample of 8 mm diameter and 20 mm long can be considered as a representative volume of the material. Before microtomographic analysis and leaching process, samples were preserved from desiccation to avoid any risk of microcracking induced by drying.

Figure 2. Different cementitious composite specimens (ϕ8 mm) after various degradation processes (leaching, thermal exposure).

The objective of experiments is to analyze different leaching states of the cementitious composite. This requires an accelerated test, able to reproduce material response that characterizes the long-term behavior of cementitious materials. The degradation process chosen for this experimental study has to fulfill the following imperative: because of time assigned for the microtomographic analysis, the material degradation must take at most 6 days. It was thus chosen, considering the geometry of the specimens, to leach the material by means of an accelerated test with ammonium nitrate solution (NH_4NO_3 – $480\ g/kg_{H2O}$). Such a leaching process has a very high kinetics (about 300 times the kinetics of leaching by deionised water) and that the ammonium nitrate-based calcium leaching leads to the same mineral end products in the cementitious material (Carde et al. 1996).

3 PRINCIPLES OF THE NUMERICAL SIMULATION

3.1 *Experimental procedure and numerical simulation*

The numerical simulation is linked to observations made on several cross-sections of a sample at different stages of leaching. The chosen cross-section has been selected because of its equal distance between the top and the bottom of the sample. The leaching front is then not influenced by end effect: the hypothesis of plane strains can be done in our calculations and would be well verified.

After a first image acquisition done on the sound sample, it has been immerged for 11 hours into the ammonium nitrate solution. This solution was regularly stirred during the total leaching period (96 h for the considered material). A new acquisition is then made, and the sample is dipped back again into the aggressive solution. New image acquisitions are performed periodically during leaching. The experimental advantage is that it is possible to compare data obtained with the same sample, making unnecessary statistical analysis. The analysis and the comparison of the various degradation stages are directly made without interference between the leaching process and the experimental device, therefore leading to accurate measurement of porosity evolution, of degradation kinetics or of the development of microcracks.

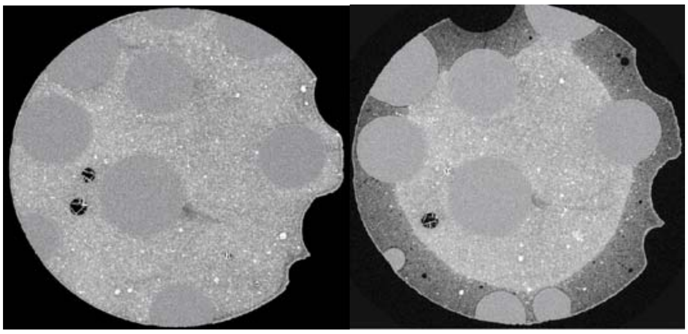

(a) (b)

Figures 3. Cross-section of the sample: (a) sound sate before leaching; (b) after 18 hours of leaching.

After numerical 3D reconstruction by back filtered projection, 3D-maps are obtained from the sample's X-ray absorption coefficient μ at different stages of leaching. The X-ray absorption coefficient is directly proportional to the density of material: dense material appears in white and porosity in black. Microcracking can be easily detected if their opening is higher than the resolution of the microtomographic analysis (here 5.1 micrometers). Any cross section through the sample can be visualized. Figure 3.a shows a cross-section of the sound sample: one can easily recognize on this picture the glass spheres and the cement matrix. On the left part of the figure, small black discs are visible: these are big porosity in which Portlandite crystals have developed. The studied cross- section has been chosen because of the geometrical distribution of the glass spheres (interactions ball-ball), and also because of the possible interaction between balls and the sample surface. In this section, the glass diameters observed are well representative of the entire sample. This cross-section is then numerically modelled: in our simulation, the glass balls and the interfaces sphere-matrix will be described, while the cement matrix is assumed homogeneous. For the sake of simplicity, all the glass spheres will not be taken into account. Figure 3.b shows the same cross-section (same distance from the sample top, Fig. 3.a) after an 18-hour period of leaching (2^{nd} step of leaching). The cement matrix is no longer homogeneous: exterior part of the sample appears darker. It is due to the decrease in calcium content and to the increase in porosity after the passage of the dissolution front (Burlion et al. 2006). Due to leaching, microcracks occur, near the glass spheres. The leaching front induces a drastic drop of cement mechanical strength: as the zones around aggregates are stressed, the decrease in tensile strength leads to microcrack openings. A numerical simulation will be performed very simply: each step of leaching is mechanically reproduced with the assumption that each leached ring (named *CP1* to *CP4* in §4.1) has its mechanical properties reduced compared to sound material.

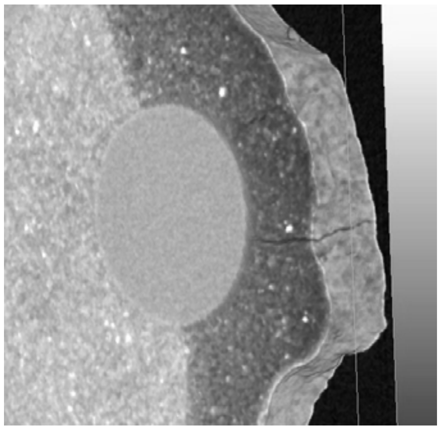

Figures 3.c. 3D-reconstruction of a slab of the leached sample during 18 hours – zoom on the right side of the figure 3.b.

An example of a 3D-reconstruction is given Figure 3.c, in which a slab (about *0.25 mm*) is presented after 18 hours of leaching. Aggregates are grey, sound cement light grey and leached cement dark grey. It is possible to distinguish the crack in 3D which connects the edge of the glass sphere at the surface sample. This crack occurs clearly during leaching process.

We have to notice that this microstructure analysis is not able to detect very small microcracks: visibility of microcracks depends on the resolution of the X-ray technique (here a pixel size of 5.1 μm), which means that cracks with width larger than 10 μm can be distinguished with certainty. Many cracks can be rather small, with a width smaller than 5 μm, and may be undetected in the present experiments.

3.2 *How to model the evolution of the leaching front?*

The finite element code used is CESAR LCPC v4, and mainly CLEO2D which solves two-dimensional problems. As mentioned previously, the hypothesis of plane strains is supposed to be verified for the studied samples.

The progression of the leaching front is numerically modelled by creating several layers in the sample. Thus, their mechanical properties will decrease gradually, taking in consideration effects of leaching process over cement paste. To remain rather qualitative than quantitative, only one leaching state has been considered. Actually, strength decrease is about *70 %* when Portlandite (Carde et al. 1996), first dissolved hydrate, disappears. Moreover, a study on accelerated leaching on mortars shows the same tendency with a dramatic decrease in physical properties (Agostini et al. 2006).

In a first approach, the cementitious matrix will be supposed to be in one of two states: sound or leached. Figure 3.b, which represents a slice of the specimen after an 18-hour leaching process, clearly shows the border between these two areas thanks to a contrast difference. The leached area is less dense than the sound one and consequently more permeable to X-ray penetration. Glass spheres, made of silica, are not degraded: their mechanical properties will remain unchanged during leaching.

3.3 *Mechanical behaviour of each constituent*

On the one hand, the constitutive law used for glass spheres (considered isotropic) is linear elastic, since stresses reached in this material in the numerical model remain in the elastic behaviour.

On the other hand, the cementitious matrix is supposed to be isotropic-elastic perfectly plastic, modelled by Mohr-Coulomb criterion. It is widely used in numerical models for many materials, such as concrete (Camborde et al. 2000).

Besides, it appears not to be mandatory to implement a strain localization limiter with Mohr-Coulomb (Gerard et al. 1998).

3.4 *Analyzed values*

At each step of leaching, the stress field and the plastic strain norm is observed and studied. It will allow to represent either preferential areas of plasticization or evolution of stresses in the sample. In addition, the cracking pattern if a damage model, where damage variables are directly linked to plastic ones (Frantziskonis & Desai 1987), had been used. Moreover, it should thus be possible to observe crack closing by means of stresses relaxation during the progression of the leaching front, particularly studying an absence of evolution of plastic strains, but a decrease in elastic strains or stresses. The norm of plastic strains $\|\varepsilon_p\|$ is defined by Equation 1.

$$\left\|\overline{\varepsilon_p}\right\| = \sqrt{\varepsilon_{Ip}{}^2 + \varepsilon_{IIp}{}^2} \quad (1)$$

where ε_{Ip} and ε_{IIp} are main plastic strains.

Analyzed stresses are the main stresses which, when $\|\varepsilon_p\| = 0$, allow to know volume variation around a node of the mesh, and so to determine whether cracks are closing or opening per Equation 2:

$$\frac{\Delta V}{V} = tr(\varepsilon_e) = \frac{(1-2\nu)(\sigma_I + \sigma_{II} + \sigma_{III})}{E}. \quad (2)$$

with ε_e the tensor of elastic strains, σ_I, σ_{II} and σ_{III} the main stresses, $\frac{\Delta V}{V}$ the volume variation, E the Young's modulus and υ the Poisson's ratio.

3.5 *Effect of maturation before leaching*

The sample is cored in a 40*40*160 mm prismatic beam that has been cured in lime-saturated water for 28 days, and then protected of desiccation for 6 months by a self-adhesive aluminium film. It is thus only submitted to endogenous shrinkage. Indeed the prismatic beam is hydraulically isolated from its environment. Measured shrinkage depends on increase in capillary pressure due to relative humidity decrease because of water consumption by not hydrated cement. Shrinkage is monitored periodically with a displacement transducer. The linear length variation which stands for linear endogenous shrinkage, supposed to be isotropic, of cement paste, is measured.

To model this effect, cement paste will be initially submitted to a thermal strain $\varepsilon_{thermal}$ equivalent to the strain caused by endogenous shrinkage $\varepsilon_{endogenous}$, the finite element code used implying this analogy explained in Equation 3 to take into account this phenomenon.

$$\varepsilon_{endogenous} \equiv \varepsilon_{thermal} = \alpha.\Delta T \quad (3)$$

where α is the thermal dilatation ratio and ΔT the equivalent thermal variation.

4 MODEL DATA

4.1 *Geometry*

The numerical sample is composed of seven spheres (#1 to #7) located as may be seen in our reference slice before leaching process (Fig. 3.a). To focus our analysis on representative cases, only these 7 aggregates have been selected, since they are representative of many geometrical disposition possibilities (Fig. 4). For instance, an aggregate far from the surface, (#7), or on the contrary close to the surface (#4 and #6), an aggregate partially out of the sample (#1, 3 and 5), neighbour aggregates (#1, 6, 2 and 3), and finally under an asperity of the surface (#2). This geometry will be adequate to simulate crack openings and besides, to extend these results to other geometrical distribution of aggregates.

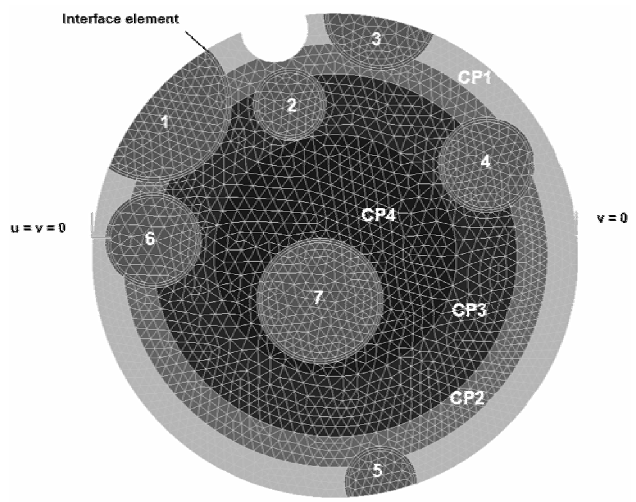

Figure 4. Mesh used in the model (u and v are respectively horizontal and vertical displacements, aggregates are numbered from *1* to *7* and cement layers from *CP1* to *CP4*).

These glass spheres are inclusions in a cementitious matrix, which has been divided up in 4 layers (approximately 1 mm-thick for *CP1* and *CP2* layers, *2 mm* for *CP3*, *CP4* being the central part of the specimen).

4.2 *Finite Element Mesh*

The generated mesh is composed of about 3,850 6-nodes triangles (quadratic interpolation). At each interface between glass aggregate and cement paste, 6-nodes interface elements are added, for a total of 151 elements. They will allow to model the interface behaviour, and as for cement paste layers, they can be sound or leached, to take into account the calcium dissolution. Indeed, the chemical composition of this interface leads to a preferential leaching process around aggregates, due to its high concentration in calcium.

4.3 *Mechanical characteristics*

Table 1 recapitulates the values of parameters that are necessary for this model: glass spheres (Bridge et al. 1983), sound and leached cement paste (Heukamp et al. 2003, Carde & Francois 1999). Internal friction angle φ is deduced from friction coefficient δ with the approximation $\delta = \sin \varphi$, C is the cohesion of the material and E its Young's modulus. The Poisson's ratio ν of the sound cement paste is 0.24, in accordance with a range of values generally reported in articles varying between 0.2 and 0.25 (Boumiz et al. 1996, Haecker et al. 2005). Due to a lack of experimental data, Poisson's ratio is assumed to be not affected by the leaching process. Intuitively, we can suppose that it will increase with degree of leaching, but it is not the hypothesis made here.

Table 1. Mechanical parameters used for each constituent.

	E (MPa)	ν	C (MPa)	φ (°)
Sound cement paste	22800	0.24	17.1	54.9
Leached cement paste	3600	0.24	1.3	34.1
Glass aggregates	73000	0.17	-	-

4.4 *Interface elements*

Interface elements allow to include in the model the paste-aggregate interface (also named Interfacial Transition Zone) which is, mechanically speaking, very weak compared to cement paste or glass. Indeed, the surface of the aggregates is smooth and rounded, avoiding creation of a strong link between these constituents, as noticed in several publications (Bisschop & van Mier 2002, Shiotani et al. 2003). Besides, glass is a non-porous material, reinforcing the interface weakness, as strong colloidal bridges are almost impossible.

That will be taken into consideration, assuming there is a Coulomb's friction at this transitional zone, with a low-value for the friction threshold. As explained previously, two cases are considered: a so-called sound interface around an aggregate when the front of leaching has not yet attacked more than half of its perimeter, and a degraded interface in the other case.

Table 2. Properties of interface elements.

	E (MPa)	f_t (MPa)	C (MPa)	φ(°)
Sound interface	14400	1,5	2	35
Leached interface	1800	1	1	25

Values for these parameters, modelling behaviour of the interface zone, are extrapolated from cement paste data obtained in the literature. Young's modulus of interface is approximately 50% lower than the matrix's (Hashin & Monteiro 2002, Yang 1998, Lutz et al. 1997). Tensile strength (f_t) is supposed to be low: 1.5 MPa, then 1 MPa after leaching. To model the weakness of the interface, and its minor contribution to the mechanical behaviour of the studied specimen, the values of the two parameters of the Coulomb friction (C and φ) are also very low. Table 2 sums up all the values of parameters used for interface elements.

Friction, separation and non-interpenetrability conditions are verified, the simulation is done for a maximum of 1000 iterations with a tolerance of 0.1% for convergence of the solution.

4.5 *Boundary conditions*

The specimen is fixed in two diametrically opposed nodes at its surface, respectively by a zero-horizontal and vertical displacement for one node, and a zero-vertical displacement for the other node. These boundary conditions well represent the specimen when it is in ammonium nitrate solution.

Besides, we can notice that the plane deformation hypothesis induces stresses in Z-axis (in the axial direction of the specimen) since axial strains are supposed to be null. These over-imposed z-stresses can be interpreted as modelling the effect of supposed other aggregates in an upper or lower section of the specimen.

4.6 *Shrinkage due to maturation*

An endogenous linear shrinkage has been measured on 40*40*160 mm prismatic specimens from which studied samples submitted to leaching have been cored. This value of -300 micro-strains is supposed isotropic. Strains due to maturation are consequently of -300 micro-strains in each direction and each point of the cement paste.

By analogy (cf. §3.6), the equivalent thermal stresses, induced by endogenous shrinkage, initially applied are modelled by a temperature variation of -30°C of the cement paste with $\alpha = 10^{-5}$ as the dilatation coefficient.

5 ANALYSIS OF NUMERICAL RESULTS

5.1 *Locations of sections*

To clearly analyse results of the simulations, we have chosen to study several sections (Fig. 5) where we will be able to observe evolutions in cement paste and glass spheres:

- in the area where the most important plastic strains are supposed to occur (sections CC' and FF')
- around an aggregate just under an asperity of the surface and close to another aggregate (section DD')
- on the surface of the sample, beginning in plain cement paste and ending close to an aggregate (section EE')
- on the surface for two aggregates close to the surface, one being an isolated aggregate (Section AA') and the other not (section BB')
- four section lines in the direction of the progression of the leaching front, one in plain cement paste far from inclusions (section JM), one in cement paste close to inclusions (aggregates #1 and #6) (section GM), and two through cement and glass aggregates (sections HM and IM)

These sections allow to study most of all existing configurations, and also to give a global view of the evolution of stresses and strains during leaching. The orientation of these sections is given by arrows as seen on the Figure 5. The origins of sections are the first point of the section (D is the origin for the section DD'), and the last point is the end of the section. For section lines, it is the same principle: M is the end of sections GM, HM, IM and JM. On curves that will be presented, the term "position on the section" stands for the X-coordinate in the local reference mark so defined and oriented.

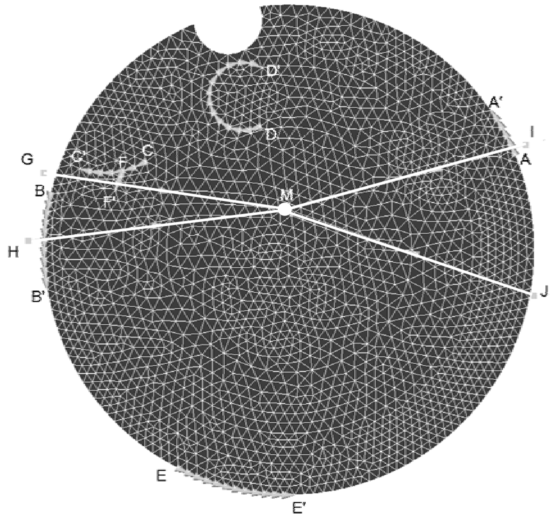

Figure 5. Localization of section lines (sections AA' to FF' and GM to JM). Arrows indicate the orientation of each section.

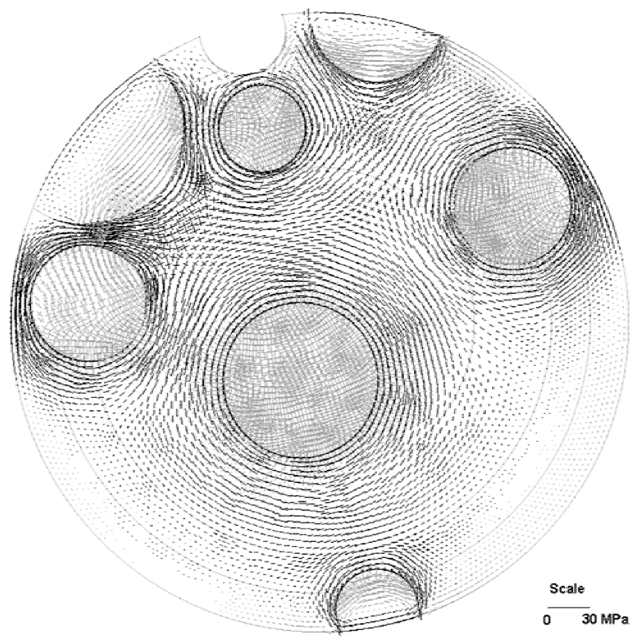

Figure 6. Representation of the main stresses in each node of the mesh (in black, tensile stress and in grey compressive stress, length of segments is proportional to intensity of stress). Axial stresses are not represented.

5.2 *Initial endogenous shrinkage*

The sound sample mature is modeled by taking into account thermal strain, which is equivalent to endogenous strain during maturation. The numerical simulation showed that, even before leaching, the sample is submitted to some severe stresses, close to the aggregates. Figure 6 shows this, representing plane main stresses in each node of the mesh. The sample, due to thermal restrain and so endogenous shrinkage, is prestressed.

An important part of the cementitious matrix is in a tensile state, since rounded aggregates avoid free shrinkage during maturation, while aggregates are in a compressive state, because of endogenous shrinkage which acts as a pressure all around them. Physically, the difference in Young's modulus between cement paste and glass explains this phenomenon. Indeed, shrinkage is higher in cement paste than in aggregates. However, there is no plastic zone in the matrix. This is a confirmation of visual observations made in Figure 3.a, where no crack can be detected at a mesoscale.

5.3 *Leaching of the first layer*

The first external layer (*CP1*, thickness = *1 mm*) is now considered as totally leached. This case corresponds to an 11-hour leaching process. Its mechanical properties are supposed uniformly degraded. Results presented further show the location of zones where plastic strains are important (Fig. 7), a darker colour meaning a higher plastic strain norm.

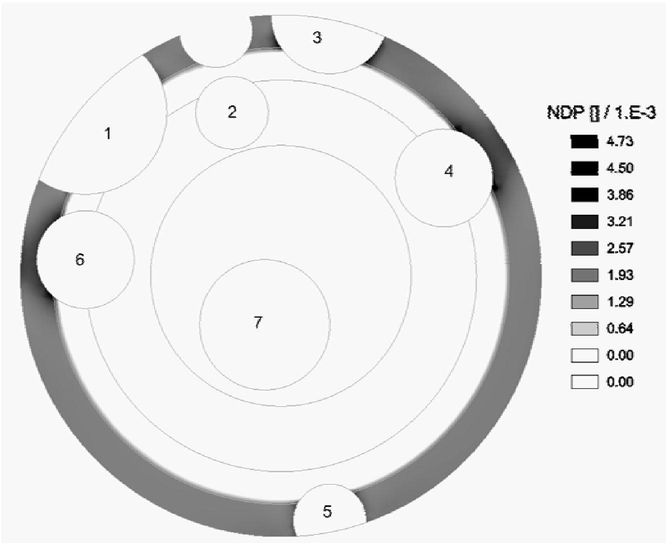

Figure 7. Isovalues of the norm of plastic strains (NDP) after leaching of the layer *CP1*. Scale is given at the right of the schema (from 0 to $4{,}73.10^{-3}$ strains).

They are located close to aggregates in the periphery of the specimen. Indeed, as underlined in the previous paragraph, the areas submitted to tension (which is the most unfavourable solicitation for cement paste) are around aggregates, where free strains are not possible. Moreover, strength of cement paste decreases with leaching, accentuating this phenomenon. So, plasticization, or damage if a damage model had been used, are mainly likely to appear in these areas.

Aggregates in subsurface of the sample (#4 and #6) are surrounded by the highest plastic strains during leaching of the first external layer. This is logical, because the thickness of the cement paste is very low.

5.4 *Leaching of the second layer*

In the same way as for leaching of the *CP1* layer, *CP2* layer is now considered as being totally leached. That corresponds to 18-hour leaching process in ammonium nitrate solution, and almost to the state observed in Figure 3.b. Figure 8 presents the cartography of plasticized zones, and mainly those close to aggregates #1, #6 and #2 which are the most interesting ones. We can already notice that, concerning crack openings, there is a concordance between numerical simulation and experimental observations on Figure 3.b. The remark (previous paragraph) as regards repartition of plasticized zones around the aggregates is confirmed by the leaching of *CP2* layer, in which the same phenomenon appears.

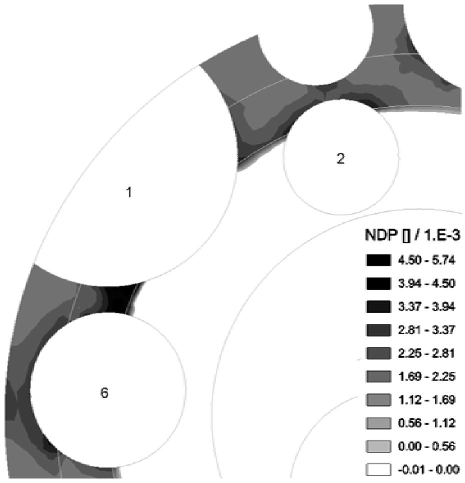

Figure 8. Isovalues of the norm of plastic strains close to aggregates #1, #2 and #6 after leaching of *CP2* layer. Each level of grey corresponds to an interval of values.

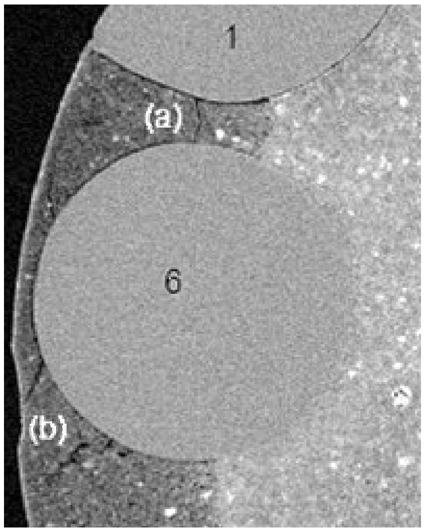

Figure 9. Zoom on aggregate #6 after an 18-hour leaching: (a) cracking between two neighbour aggregates, (b) cracking between subsurface aggregate and surface of the specimen.

A zoom onto the aggregate #6 (Fig. 9) allows to make a comparison between numerical simulation (Fig. 8) and reality obtained by means of X-ray microtomography. A good agreement exists between zones where plastic strains are important and the localization of cracks. In particular, the crack (b) of the Figure 9 perfectly coincides with numerical model (Fig. 8). In addition, if we study more precisely aggregates #1 and #6, the maximum of plastic strain deformation norm in the sample is located on the shortest distance between their surfaces (crack (a) in Figure 9). The two aggregates prevent the cement paste to freely shrink, and their proximity leads to an overlapping of the plastic areas that they each generate. This overlapping leads to a dramatic increase in values of the norm of plastic strains. If aggregates are farther from each other, plasticization becomes lower, and this could be observed looking attentively at aggregates #1 and #2, or #2 and #3 for instance.

Another remark can be drawn about occurring of plasticity close to aggregate #4 (the section IM passes through the highest area of plastic strain around aggregate #4). Indeed, propagation of plasticity begins from the surface of the aggregate, towards the periphery of the sample, and not the opposite phenomenon. This could be explained since stresses become higher as we come close to the aggregate. However, studying aggregate #6 and the section HM which passes through the diameter of the glass sphere and not through the maximum of plastic strain around it, the most important plastic strain is close to the external surface of the sample, and not around the aggregate.

6 CONCLUSIONS

In this paper, a new experimental approach to identify microcracking due to leaching of cementitious composites is presented. This technique is based on the X-ray microtomographic analysis of a sample progressively leached. We show that leaching leads to microcracking of the cement paste, particularly around rigid aggregates. This phenomenon is due to the fact that cementitious materials are auto-stressed materials due to the endogenous shrinkage. Tensile stresses occur around aggregates, then the mechanical properties of cement are reduced and lead to microcracks.

Some numerical simulations of the leaching process are performed in order to confirm this hypothesis. Experimental observations on the cement paste with glass spheres composite are confirmed by using a perfect elastoplastic model leached. As result, apparitions of high plastic strains areas are highly influenced by rounded glass aggregates, which will prevent free strains of the matrix. Moreover, the more at the surface of the specimen this aggregate is, the more important plastic strains are. High plastic strains, and so cracks, due to these rigid inclusions begin close to the aggregate surface, and then propagate inside cement paste. As a conclusion, damage modelling of leaching processes will be well adapted to numerical simulation of durability problems of concrete structures.

7 ACKNOWLEDGEMENTS

We acknowledge the European Synchrotron Radiation Facility (ESRF) for provision of synchrotron radiation facilities.

8 REFERENCES

Agostini, F. Lafhaj, Z. Skoczylas, F. & Loodsveldt, H. 2007. Experimental study of accelerated leaching on hollow cylinders of mortar, *Cement and Concrete Research* (in press)

Bisschop, J. & van Mier, J.G.M. 2002. Effect of aggregates on drying shrinkage microcracking in cement-based composites, *Materials and Structures 35*: 453-461.

Boumiz, A. Vernet, C. & Cohen Tenoudji, F. 1996. Mechanical properties of cement pastes and mortars at early ages : evolution with time and degree of hydration , *Advanced Cement Based Materials 3*: 94-106.

Burlion, N., Bernard D. & Chen D. 2006. X-ray microtomography: application to microstructure analysis of a cementitious material during leaching process, *Cement and Concrete Research 36*: 346 – 357

Bridge, B. Patel, N.D. & Waters, D.N. 1983. On the Elastic Constants and Structure of the Pure Inorganic Oxide Glasses, *Physical Status Solidi A 77*: 655.

Camborde, F. Mariotti, C. & Donzé, F.V. 2000. Numerical study of rock and concrete behaviour by discrete element modelling, *Computers and Geotechnics 27*: 225-247.

Carde, C. François, R. & Torrenti, J.M. 1996. Leaching of both calcium hydroxide and C-S-H from cement paste: modelling the mechanical behaviour, *Cement and Concrete Research 26*: 1257-1268.

Carde, C. & Francois, R. 1999. Modeling the loss of strength and porosity increase due to leaching of cement paste, *Cement and Concrete Research 21*: 181-188.

Frantziskonis, G. & Desai, C.S. 1987. Constitutive model with strain softening, *International Journal of Solids and Structures 23*: 733-750.

Gerard, B. Pijaudier-Cabot, G. & Laborderie, C. 1998. Coupled diffusion-damage modelling and the implications on failure due to strain localisation, *International Journal of Solids and Structures 35*: 4107-4120.

Haecker, C.J. Garboczi, E.J. Bullard, J.W Bohn, R.B. Sun, Z. Shah, S.P.& Voigt, T. 2005. Modeling the linear elastic properties of Portland cement paste, *Cement and Concrete Research 35*: 1948-1960.

Hashin, Z. & Monteiro, P.J.M 2002. An inverse method to determine the elastic properties of the interphase between the aggregate and the cement paste, *Cement and Concrete Research 32*: 1291–1300.

Heukamp, F.H. Ulm,F.J. & Germaine, J.T. 2003. Poroplastic properties of calcium-leached cement-based materials, *Cement and Concrete Research 33*: 1155-1173.

Lutz, M.P. Monteiro, P.J.M. & Zimmerman, R.W. 1997. Inhomogeneous interfacial transition zone model for the bulk modulus of mortar, *Cement and Concrete Research 27:* 1113-1122.

Shiotani, T. Bisschop, J. & van Mier, J.G.M. 2003 Temporal and spatial development of drying shrinkage cracking in cement-based materials, *Engineering Fracture Mechanics 70*: 1509-1525.

Yang, C.C. 1998. Effect of the transition zone on the elastic moduli of mortar, *Cement and Concrete Research 28*: 727–736.